Solid State Communications 152 (2012) 1321–1330

Contents lists available at SciVerse ScienceDirect

Solid State Communications

journal homepage: www.elsevier.com/locate/ssc

Thermal transport in graphene

Mir Mohammad Sadeghi, Michael Thompson Pettes, Li Shi *

Department of Mechanical Engineering, The University of Texas at Austin, Austin, Texas 78712, USA

ARTICLE INFO

Article history:
Accepted 12 April 2012
by L. Brey
Available online 20 April 2012

Keywords:
A. Graphene
D. Thermal conductivity
D. Phonon transport
D. Thermal interface resistance

ABSTRACT

The recent advances in graphene isolation and synthesis methods have enabled potential applications of graphene in nanoelectronics and thermal management, and have offered a unique opportunity for investigation of phonon transport in two-dimensional materials. In this review, current understanding of phonon transport in graphene is discussed along with associated experimental and theoretical investigation techniques. Several theories and experiments have suggested that the absence of interlayer phonon scattering in suspended monolayer graphene can result in higher intrinsic basal plane thermal conductivity than that for graphite. However, accurate experimental thermal conductivity data of clean suspended graphene at different temperatures are still lacking. It is now known that contact of graphene with an amorphous solid or organic matrix can suppress phonon transport in graphene, although further efforts are needed to better quantify the relative roles of interface roughness scattering and phonon leakage across the interface and to examine the effects of other support materials. Moreover, opportunities remain to verify competing theories regarding mode specific scattering mechanisms and contributions to the total thermal conductivity of suspended and supported graphene, especially regarding the contribution from the flexural phonons. Several measurements have yielded consistent interface thermal conductance values between graphene and different dielectrics and metals. A challenge has remained in establishing a comprehensive theoretical model of coupled phonon and electron transport across the highly anisotropic and dissimilar interface.
Published by Elsevier Ltd.

1. Introduction

Mechanical exfoliation of graphene from graphite onto a dielectric substrate in 2004 [1] and the subsequent reports of exceptional electrical [2,3], thermal [4,5], and mechanical properties [6] have stimulated investigations into the use of graphene for nanoelectronics [7,8] and as nanofillers to enhance the electrical [9,10] and thermal [11,12] conductivity of light-weight polymeric composites. Single-layer graphene (SLG) is a monatomic sheet of covalently bonded carbon atoms, whereas few-layer graphene (FLG) consists of several SLG sheets with van der Waals (vdW) bonding between layers. Graphene is the building block of graphite and carbon nanotubes (CNTs), with the former consisting of numerous vdW-bonded SLG sheets and the latter being SLG or FLG rolled up and joined seamlessly into a cylindrical geometry. Layer stacking is often random in natural graphite (NG), and AB ordered in highly oriented pyrolytic graphite (HOPG), also referred to as Bernal stacking [13].

These carbon allotropes possess high basal plane thermal conductivity due to strong covalent bonding, light atomic weight, and large crystalline domains. The highest room-temperature basal plane thermal conductivity (κ) of high-quality graphite is about 2000 $Wm^{-1}K^{-1}$, which was measured in pyrolytic graphite samples [14–16]. The reported κ values for individual suspended CNTs range between ~600–3000 $Wm^{-1}K^{-1}$ for single- (S) and double- (D) walled (W) CNTs [17–19] and ~40–3000 $Wm^{-1}K^{-1}$ for multi-walled (MW) CNTs [19–22]. The large variation is generally attributed to experimental uncertainties in the thermal contact resistance and CNT diameter determination, and to differences in defect concentration arising from the different synthesis methods [19]. For MWCNTs, the high temperature arc discharge and laser ablation methods yielded samples with the highest reported κ values [20,21].

Similar to graphite and CNTs, the thermal conductivity of graphene is dominated by the contribution from phonons, which are the energy quanta of lattice vibration waves, because of the much lower charge carrier density in graphene than in copper [1]. Experimentally, micro-Raman spectroscopy-based techniques [4,23–27] and micro-resistance thermometry [5,28–30] have been employed to obtain κ of graphene, in the range of 1500–5800 $Wm^{-1}K^{-1}$ for suspended SLG [4,24–27], and ~600 $Wm^{-1}K^{-1}$ for SLG supported by a SiO_2 substrate [5] at near room temperature. Meanwhile, theoretical studies on thermal transport in graphene have focused on solutions of the linearized Boltzmann transport equation (BTE) [31] and

* Corresponding author. Tel.: +1 512 471 3109; fax: +1 512 471 1045.
E-mail address: lishi@mail.utexas.edu (L. Shi).

0038-1098/$ - see front matter Published by Elsevier Ltd.
http://dx.doi.org/10.1016/j.ssc.2012.04.022

molecular dynamics (MD) simulations [32–35]. While a myriad of fundamental insights has been gained from these investigations, they have raised additional questions concerning thermal transport in these two-dimensional (2D) materials [36,37].

In this review, techniques for investigating thermal transport in graphene are examined, and the current understanding of phonon transport in graphene is summarized. Topics discussed include thermal conductivity measurement and theoretical modeling of suspended SLG, influences of contact with a dielectric, metallic, or polymeric material on phonon transport in graphene, effects of interlayer interaction on the basal-plane thermal conductivity of suspended and supported FLG, and the thermal interface resistance between graphene and various solid materials. The review is concluded with a discussion of possible future directions for further fundamental thermal transport investigations and practical thermal management applications of graphene and other 2D materials.

2. Raman thermometry measurements of graphene thermal conductivity

A Raman spectroscopy-based technique was first reported by Balandin et al. [4,38] for measuring the thermal conductivity of suspended SLG. In this measurement illustrated in Fig. 1a, a rectangular graphene flake was exfoliated from HOPG over a 2–5 μm wide trench patterned in a SiO_2 film on a silicon substrate. A 488 nm wavelength laser was focused at the center of the suspended SLG, raising its temperature locally. The Raman G peak position, calibrated versus temperature in a separate study [39], was used to determine the temperature within the irradiated region. The local temperature rise depends on the dimensions of the suspended graphene, absorbed laser power, κ of graphene, and the thermal contact resistance of the two ends of the suspended graphene. The laser power absorbed by the SLG

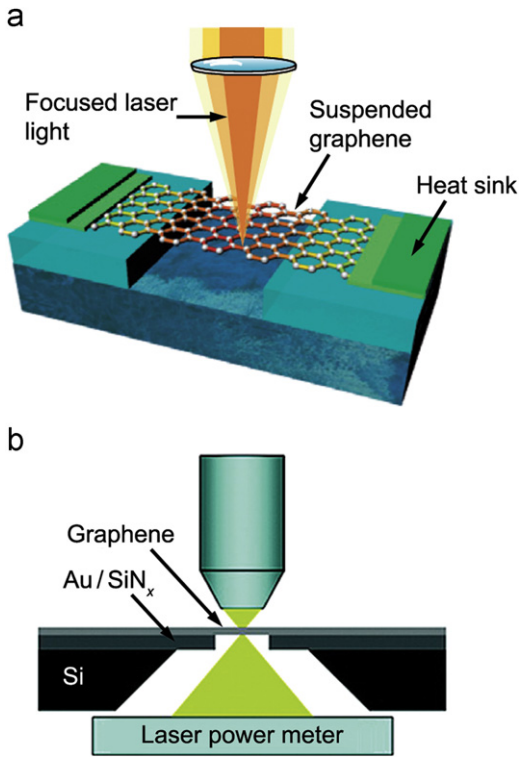

Fig. 1. (Color online) Schematic of Raman thermometry setups of (a) Balandin et al. [36] adapted with permission, copyright 2011 Nature Publishing Group, and (b) Cai et al. [25] adapted with permission, copyright 2010 American Chemical Society.

was obtained by comparing the integrated Raman intensity of the G peak with that measured on bulk HOPG. This procedure initially yielded a 13% absorption of the total laser power after two passes of the laser irradiation including the incident and reflected by the silicon substrate beneath the SLG [4]. This value was later lowered to 11–12% [38], which translates to optical absorbance of ~9% for SLG based on 0.25–0.30 reflection coefficient suggested for rough silicon in [38]. Although the experiment was conducted in ambient conditions, it was assumed that heat transfer from the SLG to the surrounding air molecules was negligible. For the supported segment of SLG, heat transfer to SiO_2 layer was neglected and the κ was assumed to be the same as that of the suspended SLG. In subsequent experiments [24], the measurement uncertainty was improved by evaporating metal heat sinks at the two ends of suspended SLG and FLG samples to reduce thermal contact resistance, and using a numerical heat conduction analysis to account for the 2D temperature distribution in the suspended graphene. From these experiments, the κ value of suspended graphene was shown to decrease with increasing layer thickness, from 3600 to 4600 $Wm^{-1}K^{-1}$ for suspended SLG to 1100–1400 $Wm^{-1}K^{-1}$ for suspended eight-layer graphene, where the observed reduction in κ was ascribed to increasing interlayer interaction [24].

Faugeras et al. [23] used the intensity ratio between the Stokes and anti-Stokes peaks, which depends on the population of optical phonons [40], to directly obtain the temperature of Raman-active optical phonons within a 632.8 nm wavelength laser spot focused at the center of a suspended SLG covering a 44 μm diameter aperture. They assumed an optical absorbance of 2.3% for the SLG exfoliated from NG based on a separate optical transmission measurement of a similar sample [41]. The temperature at the center of the SLG was optically heated to as high as about 660 K for the anti-Stokes peak intensity to become measurable. In comparison, a high-resolution spectrometer is able to resolve the small G peak shift induced by a 20–50 K temperature rise. The circular geometry of the suspended SLG in Faugeras et al.'s [23] measurements matches the radial symmetry of the laser beam, which allowed for an analytical solution of the temperature distribution to be used to determine the κ to be 632 $Wm^{-1}K^{-1}$ when the center of the SLG and substrate were at 660 K and room temperature, respectively. The different optical absorbance value used by Balandin et al. [4] was cited by Faugeras et al. [23] to explain the different measured κ values, however it is worth noting that the maximum temperature at the center of the SLG in Faugeras et al. [23] was higher than that of Balandin et al.'s work [4] and κ is expected to decreases with increasing temperature.

Cai et al. [25] directly measured the optical transmittance through SLG synthesized by chemical vapor deposition (CVD) and suspended over a 3.8 μm diameter hole. The sample was irradiated by a 532 nm wavelength laser, shown in Fig. 1b, to obtain an optical absorbance of $3.3 \pm 1.1\%$. After directly measuring the temperature dependence of the Raman G peak position, the κ value of the suspended SLG was observed to decrease from $2500+1100/-1050$ $Wm^{-1}K^{-1}$ at near room temperature to $1400+500/-480$ $Wm^{-1}K^{-1}$ at ~500 K. Additionally, the κ of the supported region of the SLG was much lower, $370+650/-320$ $Wm^{-1}K^{-1}$, attributed to the scattering of graphene phonons by the Au support.

The experiments of Balandin et al. [4], Ghosh et al. [24], Faugeras et al. [23], and Cai et al. [25] were all conducted in ambient conditions, with heat loss to the surrounding air neglected. Chen et al. [26] found that for a 9.7 μm diameter CVD SLG, the κ value obtained with the sample in air could be overestimated by 14–40% compared to the value measured in vacuum. However, the difference is comparable to the large uncertainty caused by that in the optical absorbance, determined

to be $3.4 \pm 0.7\%$ in Chen et al.'s work [26], as well as the limited temperature sensitivity of the Raman thermometry technique. Because of the large uncertainty, the measurement results were not able to verify the theoretical prediction [42] of the κ dependence on the lateral size of 2D SLG. In a subsequent report by Chen et al. [43], scattering of phonons by isotopic impurities was studied using CVD SLG, synthesized from methane with varying concentrations of ^{12}C and ^{13}C isotopes and suspended over 2.8 μm holes. The κ at 380 K was found to increase by ~36% as the isotopic purity was increased from the naturally occurring 98.9% ^{12}C to 99.9% ^{12}C.

Some of the reported κ values obtained using optothermal techniques are shown in Fig. 2. The obtained values scatter around the highest values reported for HOPG. It is worth noting that during sample preparation of Faugeras et al. [23], Cai et al. [25], and Chen et al. [26,43], the SLG was in contact with polymer resists, residuals of which are difficult to remove [44] and have been shown to strongly scatter phonons in the suspended bi-layer graphene (BLG) [30], as discussed below. In comparison, the graphene samples measured by Balandin et al. [4], Ghosh et al. [24], and Lee et al. [27] were directly exfoliated onto the measurement device, and hence are expected to be relatively clean.

Based on the above discussions, a major source of uncertainty in the Raman-based techniques lies in the very different values of optical absorbance used in different works. By measuring the optical transmittance and neglecting reflectance, in theory less than 0.1%, Nair et al. [41] obtained optical absorbance of $2.3 \pm 0.1\%$ over the wavelength range of 450–750 nm for suspended SLG. This value has been used in the optothermal measurements of Faugeras et al. [23] and Lee et al. [27]. The $3.3 \pm 1.1\%$ and $3.4 \pm 0.7\%$ values obtained by Cai et al. [25] and Chen et al. [26] suggest the large uncertainty in determining the optical absorption as the small difference between the measured incident and transmitted laser power. However, these values obtained from transmission measurements are considerably smaller than that determined by Balandin et al. [4] based on the Raman G peak intensity. Theoretically, Yang et al. [45] used first-principles calculations to show an increase of optical absorbance with decreasing wavelength due to many-electron effect. This theory was later verified experimentally by Mak et al. [46], where the optical absorbance of SLG exfoliated from Kish graphite on a SiO_2 substrate was observed to vary from ~2.3% at 1.24 μm to ~10% at 275 nm and ~3.2% at 488 nm wavelength. However, the effect of different strains between supported and suspended graphene on the optical absorbance is still unclear [47].

In addition to the uncertainty in the optical absorbance, it is unclear whether the Raman-active optical phonons are in local thermal equilibrium with acoustic phonons [40,48]. For graphene, local non-equilibrium can be caused by the very long mean free path of low-frequency phonons, which are not coupled effectively with the optical excitation or energetic charge carriers. The presence of local non-equilibrium can impose errors in the thermal conductivity result obtained from a data analysis based on Fourier's law. Furthermore, the Raman peak positions and their temperature dependence can be influenced by strains and impurity concentration in graphene [49,50]. These issues can result in errors in the measured graphene temperature and κ. In addition, due to the limited temperature sensitivity of the Raman thermometry methods, which often requires temperature rises in the suspended graphene larger than 50 K, these measurements have not been able to probe the low temperature regime, where important understandings of phonon transport physics in 2D graphene can be made.

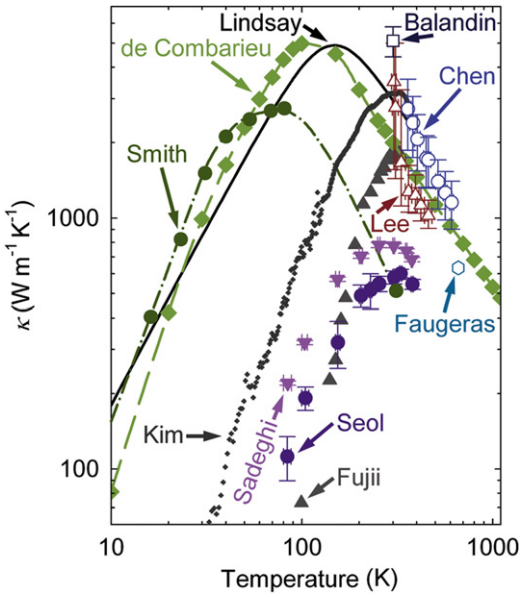

Fig. 2. (Color online) Experimental thermal conductivity (κ) of SLG exfoliated from HOPG and suspended over a 2–5 μm trench reported by Balandin et al. [4], SLG exfoliated from NG and suspended over a 44 μm diameter hole reported by Faugeras et al. [23], SLG grown by CVD and suspended over a 9.7 μm diameter hole reported by Chen et al. [26], SLG exfoliated from NG and suspended over a 6.6 μm diameter hole reported by Lee et al. [27], 9.5 μm long × 2.4 μm wide SLG exfoliated from NG and supported on SiO_2 reported by Seol et al. [5], and 12.4 μm long × 2.9 μm wide 8-layer graphene exfoliated from NG and supported on SiO_2 reported by Sadeghi and Shi [59]. Shown in comparison are the basal plane thermal conductivities of NG reported by Smith [58] and pyrolytic graphite reported by de Combarieu [15] (dash-dot and dashed lines are visual guides to the eye), a ~14 nm outer diameter, 2.5 μm long suspended MWCNT synthesized by laser ablation reported by Kim et al. [20], a 16.1 nm outer diameter, 1.89 μm long suspended MWCNT synthesized by arc discharge reported by Fujii et al. [21], and the calculated κ for a 10 μm long suspended SLG by Lindsay for Seol et al. [5] (solid line). For Raman measurement results of graphene, the temperature is the hot side temperature measured by the Raman laser, instead of the average sample temperature used in other experimental and theoretical results.

3. Micro-resistance thermometry measurements of graphene thermal conductivity

Suspended micro-resistance thermometer (RT) devices [51] have been established for thermal transport measurements of individual CNTs [17,19,20], nanowires [52–54], and nanofilms [55] covering a wide range of temperatures. The temperature sensitivity of RT devices can be made to be better than 0.05 K, up to three orders of magnitude better than that of Raman thermometry. This technique was employed by Seol et al. [5] to investigate phonon transport in 1.5–3.2 μm wide, 9.5–12.5 μm long SLG flakes exfoliated from NG onto a 300 nm thick SiO_2 bridge, which is suspended between four Cr/Au RT lines each supported by a suspended 300 nm thick SiO_2 beam, as shown in Fig. 3a. The temperatures of the four RT lines were measured when a temperature gradient was generated by electrical heating of one of the U-shape RT lines. The measurement results can be analyzed with a thermal resistance circuit to obtain the thermal conductance of the graphene/SiO_2 bridge. The thermal conductance of the SLG was determined as the drop in the bridge thermal conductance after the SLG was removed from the SiO_2 layer by oxygen plasma. Although the electron mobility of the supported SLG was determined to be similar to the highest reported values for SLG on SiO_2 [56,57], and Raman spectra indicated high sample quality, the κ of the supported SLG was reported to peak at only about 600 $Wm^{-1}K^{-1}$ at near room temperature [5]. The value is considerably lower than that reported for suspended SLG [4,25–27] and FLG [24], bulk HOPG [15,16], and bulk NG at low temperatures [58] (see Fig. 2). This

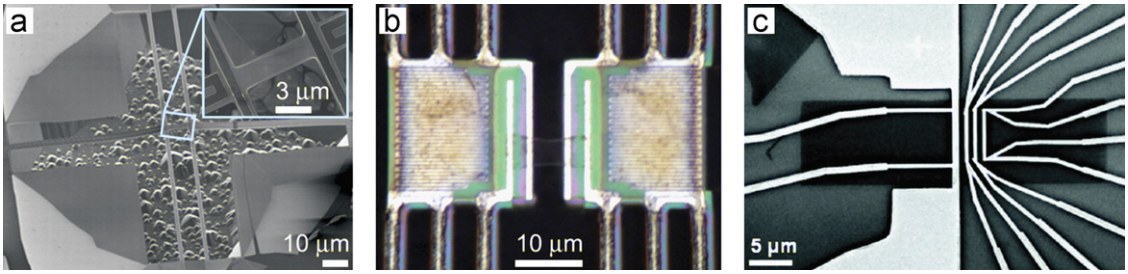

Fig. 3. (Color online) Micrographs of resistance thermometry devices of (a) Seol et al. [5] adapted with permission, copyright 2010 American Association for the Advancement of Science, (b) Pettes et al. [30] adapted with permission, copyright 2011 American Chemical Society, and (c) Jang et al. [28] reproduced with permission, copyright 2010 American Chemical Society.

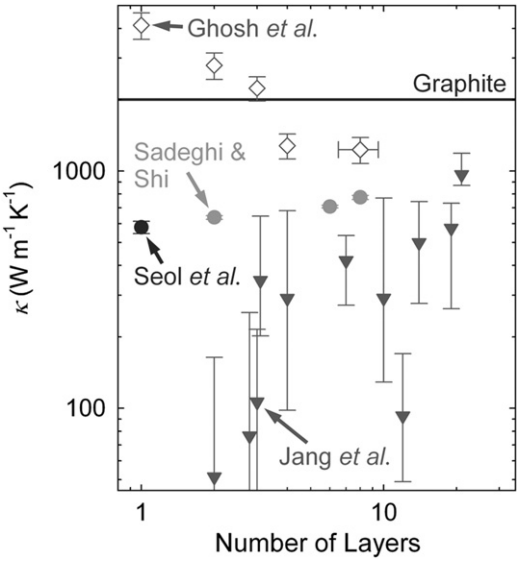

Fig. 4. Experimental thermal conductivity (κ) near room temperature of suspended SLG and FLG exfoliated from Kish graphite and suspended over 1–5 μm trenches reported by Ghosh et al. [24], SLG of Seol et al. [5] and FLG of Sadeghi and Shi [59] supported on SiO_2, and FLG encased in SiO_2 of Jang et al. [28]. Shown in comparison is the room-temperature κ of HOPG reported by de Combarieu [15].

result is in agreement with the measurement of CVD SLG on Au by Cai et al. [25], suggesting the pronounced effect of phonon-substrate interaction in supported SLG.

Pettes et al. [30] used the RT micro-device shown in Fig. 3b to find that the κ value of two suspended BLG samples was just slightly higher than that reported by Seol et al. [5] for SLG supported on SiO_2, and showed a $T^{1.5}$ dependence for temperature T below 125 K. Using a RT micro-device, Wang et al. [29] also reported low κ for a 1 μm long suspended five-layer graphene, $\sim$180 $Wm^{-1}K^{-1}$ at room temperature, as well as $\kappa \propto T^{1.5}$ dependence at low temperatures. For both works, the graphene sample was in contact with a resist layer during the sample preparation process. The transmission electron microscopy (TEM) analysis by Pettes et al. [30] revealed a thin layer of decomposed carbonaceous residue present on the BLG surface after the resist layer was dissolved and the sample was annealed at 500 °C in hydrogen. The residue was thought to scatter phonons in the suspended graphene in a similar manner as a SiO_2 support.

Jang et al. [28] patterned RT lines onto FLG encased by SiO_2 (Fig. 3c). A numerical heat transfer model was used to determine that the room-temperature κ of the embedded FLG increase from $\sim$50 $Wm^{-1}K^{-1}$ to $\sim$1000 $Wm^{-1}K^{-1}$ as the FLG thickness increased from 2 to 21 layers. Sadeghi and Shi [59], using a similar RT-based technique as Seol et al. [5], reported a similar yet less pronounced trend for FLG supported on a 300 nm thick SiO_2 film, where the room-temperature κ was observed to increase linearly from $\sim$640 $Wm^{-1}K^{-1}$ to $\sim$775 $Wm^{-1}K^{-1}$ as the FLG thickness increased from 2 to 8 layers. As shown in Fig. 4, this trend is in opposition to that reported for suspended FLG [24], indicating that substrate scattering is dominant over interlayer scattering in supported FLG. Sadeghi and Shi also found that peak of κ was shifted to lower temperatures with increasing FLG thickness, and attributed the observation to increasing phonon-substrate scattering with decreasing phonon frequency [59].

Although the experimental uncertainty is greatly improved using RT-based techniques, graphene samples used in these measurements are either supported on a substrate or contaminated by polymeric residue inherent to sample preparation. While these measurements have demonstrated that the interaction between graphene and a dielectric substrate or residual polymer can efficiently suppress phonon transport in graphene, further sensitive thermal measurements of clean suspended graphene samples are required to elucidate the intrinsic phonon transport properties of 2D graphene.

4. Theoretical models for phonon transport in graphene

A number of theoretical approaches have been reported to model phonon transport in graphene and analyze the experimental thermal conductivity data. The lattice thermal conductivity can be calculated based on the phonon dispersion and scattering rates. Fig. 5 shows that the phonon dispersion of 2D suspended SLG differs from that for HOPG with AB stacking, referred as 3D graphite. First, the unit cell size along the c-axis is 2δ for HOPG and δ for SLG, where δ is the [0002] interlayer spacing. Consequently, the primitive cell consists of four carbon atoms for HOPG and two carbon atoms for SLG. Hence, there are three acoustic and three optical phonon branches for SLG. In comparison, there are three acoustic and nine optical phonon branches for HOPG. The most notable difference is the appearance of the low-frequency out-of-plane and in-plane transverse optical branches, ZO′ and TO′, respectively, and the longitudinal optical modes, LO′, for HOPG. While the TO′ and in-plane transverse acoustic (TA) branches and the LO′ and longitudinal acoustic (LA) modes are nearly degenerate, the ZO′ and out-of-plane transverse acoustic (ZA) branches differ significantly, with the ZO′ branch exhibiting much lower phonon velocity. For HOPG, the out-of-plane transverse optical modes, ZO_1/ZO_2, is similar to that of SLG, while in-plane transverse optical modes, TO_1/TO_2, and longitudinal optical modes, LO_1/LO_2, differ from those of SLG. A detailed theoretical calculation by Lindsay et al. [60] shows that the phonon dispersions for AB stacked n-layer graphene converges to that of 3D graphite after only about five layers. Meanwhile, inelastic neutron scattering of ordered pyrolytic graphite [61] and electron energy loss spectroscopy of thin randomly stacked ‘graphite’ [62] have shown the phonon dispersion of these materials is similar to 3D graphite and 2D SLG, respectively, with

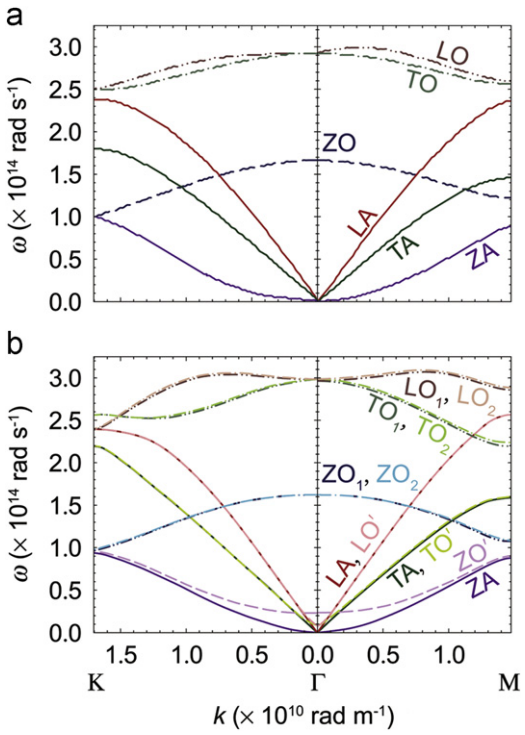

Fig. 5. (Color online) Calculated phonon dispersions for (a) graphene of Nika et al. [65] and (b) graphite of Al Jishi and Dresselhaus [66].

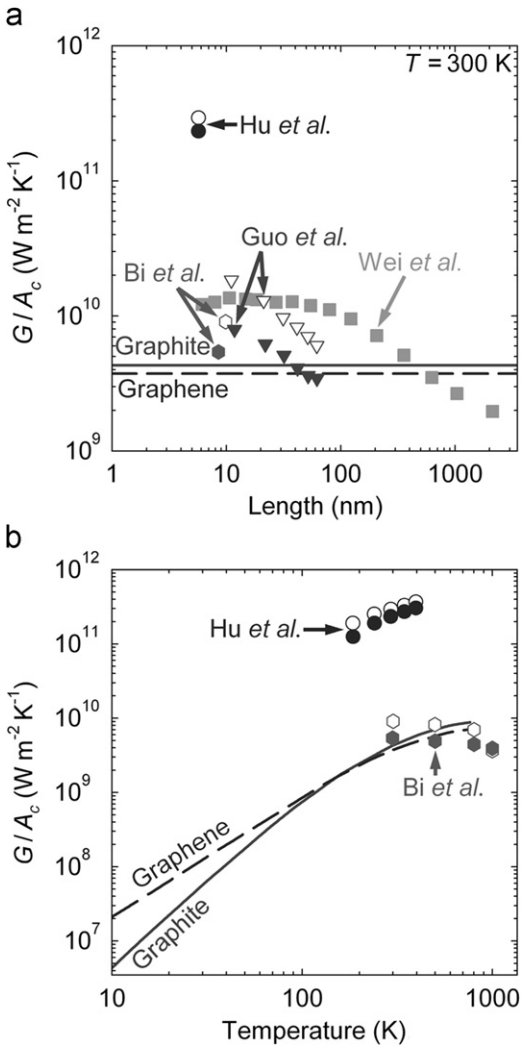

Fig. 6. The thermal conductance (G) normalized by cross-sectional area (A_c) based on SLG thickness of 0.335 nm. (a) Room-temperature results of NEMD simulations as a function of length for 5.7 nm long × 1.5 nm wide GNRs by Hu et al. [32], 2 nm wide GNRs by Guo et al. [33], ~9 nm long × ~4 nm wide GNRs by Bi et al. [34], and ~8.5 nm wide GNRs by Wei et al. [35]. (b) Temperature-dependent results of NEMD simulations by Hu et al. [32] and Bi et al. [34]. Armchair GNRs and zigzag GNRs are depicted by filled and open symbols, respectively. Shown in comparison are the calculated ballistic thermal conductance values for graphene (dashed line) and graphite (solid line) of Mingo and Broido [72].

the observation of the ZO′, TO′, and LO′ modes only in the ordered pyrolytic graphite sample. Thus, weakly interacting graphitic layers had been modeled in the literature with dispersions calculated for 2D graphene [63–65], although phonon scattering should differ between turbostratic graphite, suspended SLG [65], and HOPG [66].

In addition, although the phonon dispersion of graphene grown on Ni [62,67–69] and Ru [70] is altered by strong interaction with the metallic substrate, the acoustic phonon dispersion of graphene weakly interacting with Pt [67], Cu [68,69], Yb [68,69], La [68], and Ag [69] are similar to that calculated for suspended SLG [65,71]. Therefore, modification of the phonon dispersion is not expected to play a major role in the reduced κ observed for graphene weakly bonded by vdW force to a substrate, compared to scattering of phonons in graphene by the support.

The phonon scattering mean free path can be as long as microns in suspended SLG, especially for low-frequency (ω) phonons at low temperatures [72]. When the transport distance is smaller than the mean free path, the thermal conductance approaches the upper limit defined by the ballistic thermal conductance (G_b). The phonon contribution to G_b dominates over the electron contribution in SLG [72,73] and is shown in Fig. 6. Due to a high density of states at low-ω, the flexural phonons in the ZA branch, with quadratic dependence of frequency on wave vector, k, dominate both the specific heat, C, and G_b of SLG at low temperatures, resulting in $G_b \propto T^{1.5}$ dependence at low T. Due to the differences in phonon dispersion between SLG and graphite as discussed above, $G_b \propto T^2$ at low T for 3D graphite, and is lower than the G_b calculated for SLG at temperatures below ~150 K.

The thermal conductivity of graphene and graphite can be calculated using the Boltzmann transport equation (BTE) along with the relaxation time approximation (RTA) as [74]

$$\kappa = \frac{1}{4\pi t k_B T^2} \sum_{p=1}^{3N} \int_{k=0}^{k_{\max}} v_p^2 (\hbar\omega_p)^2 \tau_p \frac{e^{\hbar\omega_p/k_BT}}{(e^{\hbar\omega_p/k_BT}-1)^2} k\,dk, \quad (1)$$

where t is the unit cell dimension along the c-axis, δ for SLG and 2δ for 3D graphite, k_B is the Boltzmann constant, T is temperature, v_p is the phonon velocity, ω_p is the angular frequency, k is the wave vector, $\hbar$ is the reduced Planck constant, and τ_p is the relaxation time. The subscript p is used to denote each of the $3N$ individual phonon polarizations, where N is the atomic basis, 2 for SLG and 4 for 3D graphite.

Using the RTA along with the long wave approximation (LWA), Klemens and Pedraza [64] developed a model for the total relaxation time τ considering the contributions of boundary, impurity, and intrinsic phonon–phonon scattering processes. The LWA was used to describe the intrinsic relaxation lifetime τ_i arising from anharmonic three-phonon processes as

$$\tau_i^{-1} = 2\gamma^2 \frac{k_B T}{M v^2} \frac{\omega^2}{\omega_m}, \quad (2)$$

where γ, M, and ω_m are the Grüneisen parameter, atomic mass, and the maximum frequency of the acoustic mode under the Debye approximation, respectively [64]. Because of the large

lattice constant along the c-axis and the weak vdW bonding between basal planes in FLG and graphite, scattering between phonons propagating in the basal plane and those propagating along the c-axis occurs only at angular frequencies lower than $\omega_{m,c}=2.5\times10^{13}$ rad/s, the maximum frequency of the acoustic modes that propagate along the c-axis, and hence the κ contribution of phonons with $\omega<\omega_{m,c}$ was not considered in the model [64]. In the work of Klemens and Pedraza [64] for graphite, the ZA mode contribution to κ was neglected because of its low group velocity.

At high temperatures, the spectral specific heat of the phonons in the linear acoustic branches is proportional to frequency $C(\omega)\propto\omega$, whereas the phonon–phonon scattering, or intrinsic, mean free path varies as $l_i(\omega,T)\propto T^{-1}\omega^{-2}$. Hence, at high temperatures the spectral contribution to intrinsic thermal conductivity varies as $\kappa_i(\omega,T)\propto T^{-1}\omega^{-1}$ and peaks at $\omega_{m,c}$, compared to the case of a 3D isotropic crystal where $C(\omega)\propto\omega^2$, $l_i(\omega,T)\propto T^{-1}\omega^{-2}$, and $\kappa_i(T)\propto T^{-1}$. This analysis suggests that in the basal plane of graphite, phonon populations at frequencies near $\omega_{m,c}$ and with relatively long mean free paths makes the majority contribution to the total thermal conductivity.

Klemens further extended the RTA model to the thermal conductivity calculation of free-standing SLG [75,76]. Because of the absence of the interlayer coupling, which scatters low-frequency phonons in graphite, the mean free path of the low-ω phonons was only limited by the lateral dimensions (L) of clean suspended 2D SLG. Klemens ignored the thermal conductivity contribution from the low-ω phonons with $l_i>L$ by setting the lower frequency limit in the thermal conductivity integral to

$$\omega_B^2=\frac{1}{2\gamma^2}\frac{Mv^2}{k_BT}\omega_m\frac{v}{L} \tag{3}$$

Based on this model, the room-temperature thermal conductivity of free-standing SLG was predicted to increase with increasing L, from 1900 $\mathrm{Wm^{-1}K^{-1}}$ for $L=1$ μm to 5500 $\mathrm{Wm^{-1}K^{-1}}$ for $L=1$ cm. For SLG supported by a substrate with lower phonon velocities than SLG, Klemens suggested that wave energy leaking into the substrate would suppress the κ. Since phonon transmission over the interface decreases with increasing ω, the reduction is accounted for in the thermal conductivity model by ignoring the contribution of low-ω phonons with ω lower than a certain cutoff value.

Nika et al. [77] modified the model of Klemens [75,76] to consider the full phonon dispersion of graphene, instead of assuming the Debye approximation of the earlier work. Additionally, Nika et al. [65] calculated the scattering rate using phonon scattering diagrams to account for all three-phonon scattering processes that satisfy momentum and energy conservation, as opposed to the RTA of the earlier works [75–77], where the assumed three-phonon scattering phase space was not explicitly calculated. Kong et al. [78] later calculated both the phonon dispersion and the mode-dependent Grüneisen parameters from first-principles. The results were used in the RTA framework of Klemens and Pedraza [64] to calculate κ. In a more recent calculation of the κ of graphene nanoribbons, Aksamija et al. [79] considered edge roughness scattering instead of a lower cutoff frequency to limit the mean free path and prevent divergence of the thermal conductivity contribution of low-ω phonons. In these works [65,75–79], the ZA contribution to κ of suspended SLG was neglected or calculated to be negligible because of the small group velocity and large anharmonic scattering rate.

Lindsay et al. reported a numerical solution to the linearized phonon BTE to calculate the lattice thermal conductivity of SWCNTs [80] and graphene [5,31,60]. Their full quantum mechanical calculation of the phase space for three-phonon scattering processes revealed a previously ignored selection rule. As a consequence of reflection symmetry in atomically flat suspended SLG, this selection rule requires that any three-phonon scattering processes involving the ZA branch must involve an even number of ZA phonons. The limited scattering channels result in a much lower scattering rate for ZA phonons than that predicted using the RTA and LWA [64]. Because of the low scattering rate and the large density of states of ZA phonons, Lindsay et al. [5,31] calculated that ZA phonons in a 10 μm long suspended SLG with specular edges and naturally occurring isotopic concentrations should contribute as much as 77% to the total κ near room temperature, calculated to be $\sim$2950 $\mathrm{Wm^{-1}K^{-1}}$, as shown in Fig. 2. In addition, Lindsay et al. [5,31] and later Singh et al. [81] found that normal scattering processes, which are not distinguished from the umklapp processes in the RTA model, play an important role in the resultant κ of suspended SLG due to the redistribution of low-ω ZA phonons that undergo normal scattering processes.

To model the interaction between SLG and SiO_2, Seol et al. [5] used perturbation theory to investigate the phonon scattering rate due to both phonon transmission across the graphene/SiO_2 interface and local perturbation of the diagonal force constant of the graphene atoms. The scattering rate was found to rapidly increase with decreasing phonon frequency, in agreement with predictions of higher transmission for low-ω phonons across a weak vdW interface [82,83]. In this model, low-ω ZA phonons are scattered significantly by the substrate. However, this substrate scattering model has not taken into account the breaking of reflection symmetry in supported SLG, which can relax the selection rule for ZA phonon scattering and enhance scattering of ZA phonons with other phonons. The model also did not account for scattering by polymer residue that could be present on the top surface of the SLG sample.

In another investigation of the effect of interlayer interaction on the κ of SLG and FLG, Lindsay et al. [60] showed that the phase space for scattering of ZA phonon modes grows rapidly with number of graphene layers in FLG because of breaking of the reflection symmetry. The increased suppression of ZA phonons with number of graphene layers substantially reduces κ, which approaches the graphite value, $\sim$65% of the κ of SLG, after only about 5 layers. A similar conclusion was made by Singh et al. [84].

5. Molecular dynamics simulation of thermal transport in graphene

In addition to the various approximate and numerical solutions to phonon BTE, different molecular dynamics (MD) simulation approaches have been reported for investigating thermal transport in graphene. In MD simulations, atomic interaction in graphene has been treated with the Tersoff [85] or Brenner [86] potentials. Several parameters of these empirical potentials can be optimized to fit the experimental lattice constants, cohesive energy, and elastic constants. However, the obtained potentials are not necessarily optimized for phonon dispersion or thermal conductivity calculation [80]. Wei et al. [35] examined the accuracy of several empirical potentials and found that the Brenner potential is in better agreement with results from density functional theory. They also proposed another interatomic potential specifically for graphene, with parameters determined based on density functional theory calculations.

MD simulations can become extremely computationally intensive when the number of atoms in the domain is increased. Consequently, the MD computation domain has often been much smaller than the micron scale phonon–phonon scattering mean free path of low-ω phonons in suspended graphene and CNTs. Non-equilibrium (NE) MD simulations of thermal transport in

suspended graphene often require artificially enforced phonon scattering to achieve phonon equilibrium at heat baths, as well as a large temperature gradient across the domain. Such artificial boundary scattering may be avoided using periodic boundary conditions in an equilibrium (E) MD simulation based on the Green–Kubo approach [87–89], although phonon modes with wavelength larger than the domain size are still eliminated, and scattering between these low-ω phonon modes and other phonons in the domain is not accounted for [90,91]. Hence, the κ value obtained using these methods increases with increasing length [33,92,93], and the length dependence is often used to extrapolate the κ value of long graphene or CNT samples. However, for graphene nanoribbons (GNRs), where edge scattering can effectively suppress the thermal conductivity contribution from long wavelength phonons, the κ converges at a relatively short length. Haskins et al. [93] found that for an 8 nm wide GNR, convergence occurs at a length of $\sim$100 nm.

Classical MD simulation does not account for energy quantization or follow the Bose distribution of phonons, and is applicable only when the temperature is higher than the Debye temperature. However, the Debye temperature in graphene and graphite is as high as $\sim$2500 K for the in-plane acoustic modes and $\sim$1000 K for the ZA modes. Hence, new approaches for quantum correction of the MD simulation is necessary to address this issue [94].

The reported thermal conductivities using MD-based simulations range between 50 and 9000 $Wm^{-1}K^{-1}$ for a $\sim$10 nm long graphene at room temperature [32–34,95–97]. Because of the aforementioned limitations in the classical MD simulations, the quantitative κ values may not be directly comparable to experimental observations or the BTE-based models. For example, some NEMD simulations of small graphene domains or GNRs [32–35] have often yielded thermal conductance values greatly exceeding the ballistic thermal conductance, G_b [72,73], which can be calculated rather accurately based on experimentally verified phonon dispersion [63,98–100]. Such discrepancy is shown in Fig. 6. Although the ballistic thermal conductance of GNRs increases with decreasing width at low temperatures due to transition to 1D phonon density of states [101,102], the ballistic conductance calculated with the transition accounted for is still lower than some MD results. In addition, although progresses have been made to extract the phonon–phonon scattering rate from the MD results [97,103], opportunities exist in developing methods to distinguish between normal and umklapp processes.

Despite the issues regarding the accuracy of the interatomic potential, limited domain size, and the inadequacy of the classical mechanics description for lattice vibration in graphene even at room temperature, MD simulations have revealed a wealth of useful information on the relative contribution of different phonon polarizations to the total κ and the effects of substrate coupling, surface functionalization, defects, and strain. For example, considerable, but not dominant, ZA contribution to the κ of suspended SLG has been reported from MD simulations [97,104,105]. MD simulation has also predicted moderate [106] to significant [107] suppression of κ in the presence of isotopic impurities. In addition, several MD simulations [93,105,108] have reported on the extreme sensitivity of the κ of GNRs to vacancies and Stone–Wales defects [109], suggesting that a vacancy concentration as low as 0.5% can suppress the room-temperature κ of suspended SLG by 80–95%. MD simulations have also been employed to investigate the effect of mechanical strain on the κ of graphene [33,110], where both tensile and compressive strain have been predicted to suppress κ by up to $\sim$44% for $\sim$8% strain. For silicon nanowires, silicon thin films, diamond nanowires, and diamond thin films, κ increases with compressive strain due to modification of the phonon dispersion. In comparison, compressive strain in graphene induces buckling, which increases the phonon scattering rate and decreases the κ.

In addition, MD simulations have shown qualitatively that the κ of GNRs decreases by surface functionalization with hydrogen, methyl, and phenyl groups [111–113], for instance, 10% percent coverage by randomly adsorbed hydrogen was predicted to reduce κ by $\sim$70% [111]. Moreover, the EMD simulation by Qiu et al. [97] found that κ is suppressed in SLG supported on silicon due to the damping of both ZA and in-plane modes. A NEMD simulation by Ong et al. [104] showed an order of magnitude reduction in κ for SLG supported on SiO_2 compared to suspended graphene mainly due to scattering of the ZA mode. The same work predicted that increasing the interaction between SLG and the SiO_2 could increase the κ because the quadratic ZA branch was transformed to a linear branch with an increased group velocity. MD simulations of a SWCNT in a solid or liquid matrix have found that ZA phonons interact with surrounding matrix so strongly that they equilibrate with the matrix rather than SWCNT [114,115]. In another EMD simulation by Ong et al. [116], the κ of a CNT supported on SiO_2 is similar when SiO_2 atoms were either allowed to move or artificially frozen. This result suggests that scattering of CNT phonons by the interfacial bond with the substrate instead of scattering by substrate phonons is the primary cause for the $\sim$33% suppression of the κ for the supported CNT compared to a suspended CNT. Further investigations based on these approaches should be able to provide insight into the question of whether phonon leakage across the interface or roughness scattering is the main cause of the large suppression in the thermal conductivity of supported SLG compared to free-standing SLG.

6. Thermal transport across graphene interfaces

Graphene is often supported on a substrate or embedded in a medium for a number of potential applications. Consequently, a fundamental understanding of thermal transport across interfaces must be developed. Fig. 7 shows the thermal interface conductance (G_i) values between graphene and various solid materials, which have been measured using the 3ω method [117], time–domain thermoreflectance techniques [118,119], and Raman

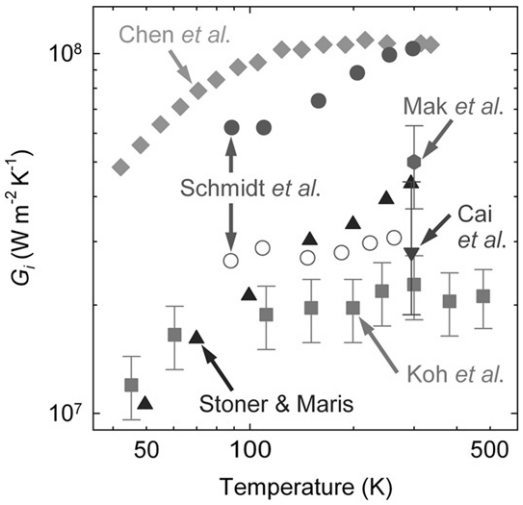

Fig. 7. Experimental thermal interface conductance (G_i) versus temperature for a 3.0 nm-thick-FLG/SiO_2 interface reported by Chen et al. [117], FLG/SiO_2 interface reported by Mak et al. [119], HOPG/Ti/Al (filled circles) and HOPG/Au (open circles) interfaces reported by Schmidt et al. [120], a SLG/Au interface reported by Cai et al. [25], a Au/Ti/three-layer grapehne/SiO_2 stack reported by Koh et al. [118], and a diamond/Au interface reported by Stoner and Maris [121].

thermometry-based methods [25]. Overall, the reported values are consistent with each other, and quantitative discrepancies are not surprising given differences in experimental techniques and sample quality. The obtained thermal interface conductance of CVD SLG/Au [25] is comparable to that of HOPG/Au [120] and diamond/Au [121]. Using the diffuse mismatch model (DMM) [122], Schmidt et al. [120] attributed the weaker temperature dependence of G_i of a HOPG/Au interface than that of a diamond/Au interface to the quasi-2D phonon density of states of HOPG.

Koh et al. [118] later showed that the G_i of Au/Ti/FLG/SiO_2 is comparable to equivalent G_i of Au/Ti/HOPG and FLG/SiO_2 stacked in series, and suggested the independence of phonon transmission across the two interfaces separated by the SLG and FLG layers. Chen et al. [117] and Mak et al. [119] also reported no dependence of the G_i value on the FLG thickness. Assuming the cross-plane κ of FLG to be similar to that of pyrolytic graphite [123–125], with a minimum value of $\sim 5\ \mathrm{Wm^{-1}\,K^{-1}}$ in the range of 50–500 K, 10-layer FLG introduces thermal resistance of less than $7\times10^{-10}\ \mathrm{m^2\,K\,W^{-1}}$ which is negligible compared to the sum of the thermal resistance values at the two interfaces, on the order of $\sim 2\times10^{-8}\ \mathrm{m^2\,K\,W^{-1}}$.

Theoretical modeling of the G_i between graphene and different materials has been reported by both MD simulations and the DMM. For the interface between graphite and an isotropic material, Duda et al. [126,127] extended the DMM to account for the anisotropy of graphite and inelastic scattering of phonons at the interface, and compared the calculation results with the experimental G_i of a HOPG/Au interface [128]. In comparison, Chen et al. [117] showed while this model without inelastic scattering modifications captures the temperature dependence of G_i of the FLG/SiO_2 interface, it underestimates the magnitude. Using NEMD, Hu et al. [129] investigated G_i of graphene in contact with an organic resin, and indicated that low-ω phonons strongly interact with the phonons of the surrounding medium and their temperature is close to the temperature of the medium instead of graphene. NEMD simulations have also been employed by Wei et al. [130] to calculate that the effective cross-plane κ of FLG increases with number of layers, as well as with temperature from 100 to 1200 K for FLG thinner than 28 layers, yet displays a peak at $\sim$400 K for 48-layer thick FLG. In comparison, the cross-plane κ of graphite shows a peak at about 30 K [16]. The predicted increase in the temperature of the peak κ with decreasing thickness is expected due to phonon-boundary scattering at heat baths.

7. Summary and outlook

A number of the large body of reported experimental and theoretical studies of thermal transport in and across graphene have been discussed in the preceding sections. Results from several Raman thermometry-based techniques have suggested that the basal plane κ of suspended graphene may exceed that of graphite and diamond. However, interpretations of these experiments are complicated by uncertainty in the optical absorption, strain-induced effects on the Raman spectra, questions regarding the local equilibrium between low-ω acoustic phonons and the Raman active optical phonons, and limited temperature sensitivity. Micro-resistance thermometry-based techniques have provided superior temperature sensitivity, allowing investigations of the low-temperature thermal transport processes, and have revealed pronounced phonon–substrate interaction in graphene in contact with a dielectric or polymeric layer. Given the limitations of existing experimental techniques for studying thermal transport in graphene, novel experimental techniques for probing phonon-transport in clean suspended graphene would be very helpful to address a number of outstanding fundamental questions.

One of the outstanding questions is the contribution of different phonon polarizations to the thermal conductivity. The flexural phonon contribution to the thermal conductivity of graphene is negligible based on a RTA approach, and is dominant according to a numerical solution of the phonon BTE and full quantum mechanical calculation of the phonon–phonon scattering phase space. In comparison, EMD simulations have predicted that the ZA contribution is neither negligible nor dominant in suspended graphene near room temperature. While MD simulations have provided valuable qualitative insights, the limited computation domain size and classical nature of MD simulations will need to be addressed for the MD results to be compared meaningfully with other theoretical predictions and experimental results. Further theoretical investigations may lead to better understating of the actual contribution of the ZA modes in both suspended and supported graphene, and the respective roles of roughness scattering and phonon leakage in reducing the κ of supported and embedded graphene.

The measured thermal interface resistance values between graphene and different materials have been relatively consistent between different measurements, compared to the large variation in the experimental in-plane κ data. Although progress has also been made in the theoretical modeling of phonon transport across the interface between graphene and another material, this is an area worthy of further study owing to the lack of detailed understanding of the interface structure, as well as intriguing questions regarding inelastic scattering and electron–phonon coupling at the interface.

These fundamental thermal transport studies are highly relevant to the performance and reliability of graphene electronic devices and the applications of graphene for thermal management. Although the small cross section of SLG limits its thermal conductance value despite its high thermal conductivity even with a support layer, the high surface to volume ratio is desirable for its use as nanofillers to enhance the thermal conductivity of polymer composites. It has been reported that graphene–polymeric composites can show larger thermal conductivity enhancement than CNT–polymer composites because of the 2D geometry [12,131]. However, the performance is limited by the interface thermal resistance between percolated nanofillers. The recently reported foam architecture of few layer graphene and ultrathin graphite [10] potentially provides a solution to the interface thermal resistance bottleneck, and leads to further thermal conductivity enhancement in graphene foam–polymer composites. It has also been suggested that FLG may be used as a lateral heat spreader in high-power density nanoelectronic devices. For this purpose as well as heat spreading in flexible electronic devices, the heat spreading layer often needs to be electrically isolated from the active device layer. Hence, few-layer hexagonal boron nitride (h-BN) may be favorable because of the large bandgap, high thermal conductivity, and similar crystal structure of this dielectric to electrically-conducting graphene. Hence, besides the aforementioned outstanding fundamental questions regarding graphene, abundant opportunities exist in investigations of thermal transport in other 2D materials as well as 3D architectures of 2D building blocks.

Acknowledgments

The authors' research in related areas has been supported by National Science Foundation Thermal Transport Processes Program, Office of Basic Energy Science and ARPA-E of Department of Energy, and Office of Naval Research.

References

[1] K.S. Novoselov, A.K. Geim, S.V. Morozov, D. Jiang, Y. Zhang, S.V. Dubonos, I.V. Grigorieva, A.A. Firsov, Science 306 (2004) 666.

[2] K.I. Bolotin, K.J. Sikes, Z. Jiang, M. Klima, G. Fudenberg, J. Hone, P. Kim, H.L. Stormer, Solid State Commun. 146 (2008) 351.
[3] X. Du, I. Skachko, A. Barker, E.Y. Andrei, Nat. Nanotechnol. 3 (2008) 491.
[4] A.A. Balandin, S. Ghosh, W.Z. Bao, I. Calizo, D. Teweldebrhan, F. Miao, C.N. Lau, Nano Lett. 8 (2008) 902.
[5] J.H. Seol, I. Jo, A.L. Moore, L. Lindsay, Z.H. Aitken, M.T. Pettes, X.S. Li, Z. Yao, R. Huang, D. Broido, N. Mingo, R.S. Ruoff, L. Shi, Science 328 (2010) 213.
[6] C. Lee, X. Wei, J.W. Kysar, J. Hone, Science 321 (2008) 358.
[7] Y.M. Lin, C. Dimitrakopoulos, K.A. Jenkins, D.B. Farmer, H.Y. Chiu, A. Grill, P. Avouris, Science 327 (2010) 662.
[8] F. Schwierz, Nat. Nanotechnol. 5 (2010) 487.
[9] S. Stankovich, D.A. Dikin, G.H.B. Dommett, K.M. Kohlhaas, E.J. Zimney, E.A. Stach, R.D. Piner, S.T. Nguyen, R.S. Ruoff, Nature 442 (2006) 282.
[10] Z.P. Chen, W.C. Ren, L.B. Gao, B.L. Liu, S.F. Pei, H.M. Cheng, Nat. Mater. 10 (2011) 424.
[11] F. Yavari, H.R. Fard, K. Pashayi, M.A. Rafiee, A. Zamiri, Z.Z. Yu, R. Ozisik, T. Borca-Tasciuc, N. Koratkar, J. Phys. Chem. C 115 (2011) 8753.
[12] K.M.F. Shahil, A.A. Balandin, Nano Lett. 12 (2012) 861.
[13] J.D. Bernal, Proc. R. Soc. London A 106 (1924) 749.
[14] J.C. Bowman, J.A. Krumhansl, J.T. Meers, Ind. Carbon Graphite (1958) 52.
[15] A. de Combarieu, Bull. Inst. Intern. Froid. Annexe 2 (1965) 63.
[16] Y.S. Touloukian, R.W. Powell, C.Y. Ho, P.G. Klemens, Thermal conductivity—nonmetallic solids, in: Y.S. Touloukian, C.Y. Ho (Eds.), Thermophysical Properties of Matter, IFI/Plenum, New York, 1970.
[17] C.H. Yu, L. Shi, Z. Yao, D.Y. Li, A. Majumdar, Nano Lett. 5 (2005) 1842.
[18] E. Pop, D. Mann, Q. Wang, K. Goodson, H.J. Dai, Nano Lett. 6 (2006) 96.
[19] M.T. Pettes, L. Shi, Adv. Funct. Mater. 19 (2009) 3918.
[20] P. Kim, L. Shi, A. Majumdar, P.L. McEuen, Phys. Rev. Lett. 87 (2001) 215502.
[21] M. Fujii, X. Zhang, H.Q. Xie, H. Ago, K. Takahashi, T. Ikuta, H. Abe, T. Shimizu, Phys. Rev. Lett. 95 (2005) 065502.
[22] T.Y. Choi, D. Poulikakos, J. Tharian, U. Sennhauser, Nano Lett. 6 (2006) 1589.
[23] C. Faugeras, B. Faugeras, M. Orlita, M. Potemski, R.R. Nair, A.K. Geim, ACS Nano 4 (2010) 1889.
[24] S. Ghosh, W.Z. Bao, D.L. Nika, S. Subrina, E.P. Pokatilov, C.N. Lau, A.A. Balandin, Nat. Mater. 9 (2010) 555.
[25] W.W. Cai, A.L. Moore, Y.W. Zhu, X.S. Li, S.S. Chen, L. Shi, R.S. Ruoff, Nano Lett. 10 (2010) 1645.
[26] S.S. Chen, A.L. Moore, W.W. Cai, J.W. Suk, J.H. An, C. Mishra, C. Amos, C.W. Magnuson, J.Y. Kang, L. Shi, R.S. Ruoff, ACS Nano 5 (2011) 321.
[27] J.U. Lee, D. Yoon, H. Kim, S.W. Lee, H. Cheong, Phys. Rev. B 83 (2011) 081419. R.
[28] W.Y. Jang, Z. Chen, W.Z. Bao, C.N. Lau, C. Dames, Nano Lett. 10 (2010) 3909.
[29] Z.Q. Wang, R.G. Xie, C.T. Bui, D. Liu, X.X. Ni, B.W. Li, J.T.L. Thong, Nano Lett. 11 (2011) 113.
[30] M.T. Pettes, I.S. Jo, Z. Yao, L. Shi, Nano Lett. 11 (2011) 1195.
[31] L. Lindsay, D.A. Broido, N. Mingo, Phys. Rev. B 82 (2010) 115427.
[32] J.N. Hu, X.L. Ruan, Y.P. Chen, Nano Lett. 9 (2009) 2730.
[33] Z.X. Guo, D. Zhang, X.G. Gong, Appl. Phys. Lett. 95 (2009) 163103.
[34] K.D. Bi, Y.F. Chen, M.H. Chen, Y.J. Wang, Solid State Commun. 150 (2010) 1321.
[35] D.S. Wei, Y. Song, F. Wang, J. Chem. Phys. 134 (2011) 184704.
[36] A.A. Balandin, Nat. Mater. 10 (2011) 569.
[37] L. Shi, Nanoscale & Microscale Thermophys. Eng., http://dx.doi.org/10.1080/15567265.2012.667514, in press.
[38] S. Ghosh, I. Calizo, D. Teweldebrhan, E.P. Pokatilov, D.L. Nika, A.A. Balandin, W. Bao, F. Miao, C.N. Lau, Appl. Phys. Lett. 92 (2008) 151911.
[39] I. Calizo, A.A. Balandin, W. Bao, F. Miao, C.N. Lau, Nano Lett. 7 (2007) 2645.
[40] S. Berciaud, M.Y. Han, K.F. Mak, L.E. Brus, P. Kim, T.F. Heinz, Phys. Rev. Lett. 104 (2010) 227401.
[41] R.R. Nair, P. Blake, A.N. Grigorenko, K.S. Novoselov, T.J. Booth, T. Stauber, N.M.R. Peres, A.K. Geim, Science 320 (2008) 1308.
[42] S. Lepri, R. Livi, A. Politi, Phys. Rep. 377 (2003) 1.
[43] S. Chen, Q. Wu, C. Mishra, J. Kang, H. Zhang, K. Cho, W. Cai, A.A. Balandin, R.S. Ruoff, Nat. Mater. 11 (2012) 203.
[44] Y.C. Lin, C.C. Lu, C.H. Yeh, C.H. Jin, K. Suenaga, P.W. Chiu, Nano Lett. 12 (2012) 414.
[45] L. Yang, J. Deslippe, C.H. Park, M.L. Cohen, S.G. Louie, Phys. Rev. Lett. 103 (2009) 186802.
[46] K.F. Mak, J. Shan, T.F. Heinz, Phys. Rev. Lett. 106 (2011) 046401.
[47] F.M.D. Pellegrino, G.G.N. Angilella, R. Pucci, Phys. Rev. B 81 (2010) 035411.
[48] D.H. Chae, B. Krauss, K. von Klitzing, J.H. Smet, Nano Lett. 10 (2010) 466.
[49] A. Das, S. Pisana, B. Chakraborty, S. Piscanec, S.K. Saha, U.V. Waghmare, K.S. Novoselov, H.R. Krishnamurthy, A.K. Geim, A.C. Ferrari, A.K. Sood, Nat. Nanotechnol. 3 (2008) 210.
[50] D.M. Basko, S. Piscanec, A.C. Ferrari, Phys. Rev. B 80 (2009) 165413.
[51] L. Shi, D.Y. Li, C.H. Yu, W.Y. Jang, D. Kim, Z. Yao, P. Kim, A. Majumdar, J. Heat Transfer 125 (2003) 881.
[52] F. Zhou, J. Szczech, M.T. Pettes, A.L. Moore, S. Jin, L. Shi, Nano Lett. 7 (2007) 1649.
[53] A. Mavrokefalos, A.L. Moore, M.T. Pettes, L. Shi, W. Wang, X.G. Li, J. Appl. Phys. 105 (2009) 104318.
[54] A.L. Moore, M.T. Pettes, F. Zhou, L. Shi, J. Appl. Phys. 106 (2009) 034310.
[55] A. Mavrokefalos, M.T. Pettes, F. Zhou, L. Shi, Rev. Sci. Instrum. 78 (2007) 034901.
[56] Y.W. Tan, Y. Zhang, K. Bolotin, Y. Zhao, S. Adam, E.H. Hwang, S. Das Sarma, H.L. Stormer, P. Kim, Phys. Rev. Lett. 99 (2007) 246803.
[57] J.H. Chen, C. Jang, S. Xiao, M. Ishigami, M.S. Fuhrer, Nat. Nanotechnol. 3 (2008) 206.
[58] A.W. Smith, Phys. Rev. 95 (1954) 1095.
[59] M.M. Sadeghi, L. Shi, in: Proceedings of the 2011 ASME International Mechanical Engineering Congress and Exposition, Denver, Colorado, USA, 2011, pp. 64227.
[60] L. Lindsay, D.A. Broido, N. Mingo, Phys. Rev. B 83 (2011) 235428.
[61] R. Nicklow, H.G. Smith, N. Wakabaya, Phys. Rev. B 5 (1972) 4951.
[62] T. Aizawa, R. Souda, S. Otani, Y. Ishizawa, C. Oshima, Phys. Rev. B 42 (1990) 11469.
[63] R.A. Jishi, L. Venkataraman, M.S. Dresselhaus, G. Dresselhaus, Chem. Phys. Lett. 209 (1993) 77.
[64] P.G. Klemens, D.F. Pedraza, Carbon 32 (1994) 735.
[65] D.L. Nika, E.P. Pokatilov, A.S. Askerov, A.A. Balandin, Phys. Rev. B 79 (2009) 155413.
[66] R. Al-Jishi, G. Dresselhaus, Phys. Rev. B 26 (1982) 4514.
[67] T. Aizawa, Y. Hwang, W. Hayami, R. Souda, S. Otani, Y. Ishizawa, Surf. Sci. 260 (1992) 311.
[68] A.M. Shikin, D. Farias, V.K. Adamchuk, K.H. Rieder, Surf. Sci. 424 (1999) 155.
[69] D. Farias, K.H. Rieder, A.M. Shikin, V.K. Adamchuk, T. Tanaka, C. Oshima, Surf. Sci. 454 (2000) 437.
[70] M.C. Wu, Q. Xu, D.W. Goodman, J. Phys. Chem. 98 (1994) 5104.
[71] A. Allard, L. Wirtz, Nano Lett. 10 (2010) 4335.
[72] N. Mingo, D.A. Broido, Phys. Rev. Lett. 95 (2005) 096105.
[73] K. Saito, J. Nakamura, A. Natori, Phys. Rev. B 76 (2007) 115409.
[74] G. Chen, Nanoscale Energy Transport and Conversion: A Parallel Treatment of Electrons, Molecules, Phonons, and Photons, Oxford University Press, New York, 2005.
[75] P.G. Klemens, J. Wide Bandgap Mater. 7 (2000) 332.
[76] P.G. Klemens, Int. J. Thermophys. 22 (2001) 265.
[77] D.L. Nika, S. Ghosh, E.P. Pokatilov, A.A. Balandin, Appl. Phys. Lett. 94 (2009) 203103.
[78] B.D. Kong, S. Paul, M.B. Nardelli, K.W. Kim, Phys. Rev. B 80 (2009) 033406.
[79] Z. Aksamija, I. Knezevic, Appl. Phys. Lett. 98 (2011) 141919.
[80] L. Lindsay, D.A. Broido, N. Mingo, Phys. Rev. B 80 (2009) 125407.
[81] D. Singh, J.Y. Murthy, T.S. Fisher, J. Appl. Phys. 110 (2011) 113510.
[82] R. Prasher, Appl. Phys. Lett. 94 (2009) 041905.
[83] M. Schoenberg, J. Acoust. Soc. Am. 68 (1980) 1516.
[84] D. Singh, J.Y. Murthy, T.S. Fisher, J. Appl. Phys. 110 (2011) 044317.
[85] J. Tersoff, Phys. Rev. B 39 (1989) 5566.
[86] D.W. Brenner, O.A. Shenderova, J.A. Harrison, S.J. Stuart, B. Ni, S.B. Sinnott, J. Phys.: Condens. Matter 14 (2002) 783.
[87] M.S. Green, J. Chem. Phys. 20 (1952) 1281.
[88] R. Kubo, J. Phys. Soc. Jpn. 12 (1957) 570.
[89] R. Kubo, M. Yokota, S. Nakajima, J. Phys. Soc. Jpn. 12 (1957) 1203.
[90] D.P. Sellan, E.S. Landry, J.E. Turney, A.J.H. McGaughey, C.H. Amon, Phys. Rev. B 81 (2010) 214305.
[91] S.G. Volz, G. Chen, Phys. Rev. B 61 (2000) 2651.
[92] P.K. Schelling, S.R. Phillpot, P. Keblinski, Phys. Rev. B 65 (2002) 144306.
[93] J. Haskins, A. Kinaci, C. Sevik, H. Sevincli, G. Cuniberti, T. Cagin, ACS Nano 5 (2011) 3779.
[94] J.E. Turney, A.J.H. McGaughey, C.H. Amon, Phys. Rev. B 79 (2009) 139.
[95] S. Berber, Y.K. Kwon, D. Tomanek, Phys. Rev. Lett. 84 (2000) 4613.
[96] W.J. Evans, L. Hu, P. Keblinski, Appl. Phys. Lett. 96 (2010) 203112.
[97] B. Qiu, X. Ruan, arXiv:1111.4613v1 (2011).
[98] N. Mounet, N. Marzari, Phys. Rev. B 71 (2005) 205214.
[99] C. Oshima, T. Aizawa, R. Souda, Y. Ishizawa, Y. Sumiyoshi, Solid State Commun. 65 (1988) 1601.
[100] S. Siebentritt, R. Pues, K.H. Rieder, A.M. Shikin, Phys. Rev. B 55 (1997) 7927.
[101] J.W. Jiang, J.S. Wang, B.W. Li, Phys. Rev. B 79 (2009) 205418.
[102] E. Munoz, J.X. Lu, B.I. Yakobson, Nano Lett. 10 (2010) 1652.
[103] J.A. Thomas, J.E. Turney, R.M. Iutzi, C.H. Amon, A.J.H. McGaughey, Phys. Rev. B 81 (2010) 081411. (R).
[104] Z.Y. Ong, E. Pop, Phys. Rev. B 84 (2011) 075471.
[105] H.J. Zhang, G. Lee, K. Cho, Phys. Rev. B 84 (2011) 115460.
[106] J.N. Hu, S. Schiffli, A. Vallabhaneni, X.L. Ruan, Y.P. Chen, Appl. Phys. Lett. 97 (2010) 133107.
[107] J.W. Jiang, J.H. Lan, J.S. Wang, B.W. Li, J. Appl. Phys. 107 (2010) 054314.
[108] F. Hao, D.N. Fang, Z.P. Xu, Appl. Phys. Lett. 99 (2011) 041901.
[109] A.J. Stone, D.J. Wales, Chem. Phys. Lett. 128 (1986) 501.
[110] X.B. Li, K. Maute, M.L. Dunn, R.G. Yang, Phys. Rev. B 81 (2010) 245318.
[111] S.K. Chien, Y.T. Yang, C.K. Chen, Appl. Phys. Lett. 98 (2011) 033107.
[112] Q.X. Pei, Z.D. Sha, Y.W. Zhang, Carbon 49 (2011) 4752.
[113] S.K. Chien, Y.T. Yang, C.K. Chen, Carbon 50 (2012) 421.
[114] C.F. Carlborg, J. Shiomi, S. Maruyama, Phys. Rev. B 78 (2008) 205406.
[115] S. Shenogin, L.P. Xue, R. Ozisik, P. Keblinski, D.G. Cahill, J. Appl. Phys. 95 (2004) 8136.
[116] Z.Y. Ong, E. Pop, J. Shiomi, Phys. Rev. B 84 (2011) 165418.
[117] Z. Chen, W. Jang, W. Bao, C.N. Lau, C. Dames, Appl. Phys. Lett. 95 (2009) 161910.
[118] Y.K. Koh, M.H. Bae, D.G. Cahill, E. Pop, Nano Lett. 10 (2010) 4363.
[119] K.F. Mak, C.H. Lui, T.F. Heinz, Appl. Phys. Lett. 97 (2010) 221904.
[120] A.J. Schmidt, K.C. Collins, A.J. Minnich, G. Chen, J. Appl. Phys. 107 (2010) 104907.
[121] R.J. Stoner, H.J. Maris, Phys. Rev. B 48 (1993) 16373.
[122] E.T. Swartz, R.O. Pohl, Rev. Mod. Phys. 61 (1989) 605.
[123] J. Pappis, S.L. Blum, J. Am. Ceram. Soc. 44 (1961) 592.

[124] C.N. Hooker, A.R. Ubbelohde, D.A. Young, Proc. R. Soc. London A 276 (1963) 83.
[125] C.A. Klein, M.G. Holland, Phys. Rev. 136 (1964) A575.
[126] J.C. Duda, J.L. Smoyer, P.M. Norris, P.E. Hopkins, Appl. Phys. Lett. 95 (2009) 031912.
[127] J.C. Duda, P.E. Hopkins, T.E. Beechem, J.L. Smoyer, P.M. Norris, Superlattices Microstruct. 47 (2010) 550.
[128] P.M. Norris, J.L. Smoyer, J.C. Duda, P.E. Hopkins, J. Heat Transfer 134 (2012) 020910.
[129] L. Hu, T. Desai, P. Keblinski, Phys. Rev. B 83 (2011) 195423.
[130] Z.Y. Wei, Z.H. Ni, K.D. Bi, M.H. Chen, Y.F. Chen, Phys. Lett. A 375 (2011) 1195.
[131] C.W. Nan, R. Birringer, D.R. Clarke, H. Gleiter, J. Appl. Phys. 81 (1997).